Relating P-Band Synthetic Aperture Radar Tomography to Tropical Forest Biomass

Dinh Ho Tong Minh, Thuy Le Toan, Fabio Rocca, Stefano Tebaldini,
Mauro Mariotti d'Alessandro, and Ludovic Villard

Manuscript received March 7, 2012; revised December 20, 2012; accepted February 2, 2013. Date of publication March 27, 2013; date of current version December 12, 2013.

D. Ho Tong Minh, F. Rocca, S. Tebaldini, and M. Mariotti d'Alessandro are with the Dipartimento di Elettronica e Informazione, Politecnico di Milano, Milano 20133, Italy (e-mail: htmdinh@elet.polimi.it; rocca@elet.polimi.it; tebaldini@elet.polimi.it; mariotti.dalessandro@elet.polimi.it).

T. Le Toan and L. Villard are with the Centre d'Etudes Spatiales de la Biosphere (CESBIO), Toulouse 31000, France, (e-mail: thuy.letoan@cesbio.cnes.fr; ludovic.villard@cesbio.cnes.fr).

Color versions of one or more of the figures in this paper are available online.

I. Introduction

FORESTS cover almost one-third of the earth's surface and are recognized to have an impact on the global climate of the planet. Considering only tropical regions, deforestation accounts for up to 20% of the carbon dioxide (CO_2) emitted by humanity each year. Besides that, forests also contribute to carbon sequestration, which is carbon removed from the atmosphere through the vegetation growth process. However, there is still great uncertainty about the exact role of forests in the carbon cycle, as for both the spatial distribution of carbon stocks and carbon exchange and in the estimates of carbon emissions [1]–[4]. Forest biomass represents a key parameter in the assessment of terrestrial carbon budget [5]. Yet, forest biomass is poorly quantified at a global scale, due to the great difficulty in measuring biomass on the ground and aggregating measurements across scales.

The urgency to deliver accurate maps of forest biomass at a global scale was one of the main reasons behind the proposal of BIOMASS as the European Space Agency's (ESA's) seventh Earth Explorer mission. BIOMASS can be implemented as a synthetic aperture radar (SAR), aimed at providing maps of forest above-ground biomass (AGB) twice a year over the life of the five-year mission at 20% accuracy. The SAR system will yield fully polarimetric measurements at P-band (435 MHz), so as to take advantage of the under-foliage penetration capabilities of long wavelengths.[1] The algorithms to be employed for AGB retrieval have been developed during Phase-A BIOMASS activities, employing data collected over boreal and tropical forests. These algorithms can be divided into two main classes [6].

1) AGB estimation from polarimetric intensities (PolSAR): this class of algorithms combines statistical and physical concepts to develop regressions between AGB and intensity measurements in all polarizations [6]–[9]. These algorithms performed well for temperate and boreal forests for which the AGB is less than about 300 t ha^{-1}. Beyond 300 t ha^{-1}, the sensitivity of the backscattered intensity to AGB decreases drastically, and is often obscured by various noise sources, the most important being uncertainties in radar and *in situ* AGB measurements, and topographic effects. This is referred to as the saturation effect [10]. The retrieval of AGB of dense tropical forest with AGB up to 500 t ha^{-1} is thus recognized as a challenging task.
2) AGB estimation from polarimetric SAR Interferometry (PolInSAR): PolInSAR techniques allow us to estimate forest height by combining two PolSAR measurements

[1] P-band is *de facto* the lowest frequency band employable by a spaceborne radar for earth observation, due to ionospheric distortions and International Telecommunication Union (ITU) regulations.

from slightly different orbits [11]. Forest height estimates are then converted to AGB using allometric equations [3], [12]–[15]. The information about forest height is expected to be useful at high biomass values, as it helps mitigate intensity saturation phenomena.

The two approaches can then be combined using a minimum square error approach to yield a final AGB estimate [6]. As reported in [6], the combined approach is expected to be able to generate AGB maps to about or within the desired 20% for boreal and tropical forests. To achieve this performance, however, AGB estimation algorithms need to be accurately tuned, so as to take into account disturbing factors affecting radar measurements, which are primarily terrain topography and variations in the forest vertical structure [6]. Terrain topography represents one important disturbing factor, as it can affect significantly the magnitude of returns from trunk–ground and branch–ground double-bounce interactions [16]–[19], resulting in variations of the observed signal that are not correlated to forest biomass. Forest vertical structure determines a variation of the distribution of the backscattered power in the three polarizations as well as the interferometric coherence between different acquisitions, resulting in a possible source of error for forest height estimates to be employed for AGB estimation.[2] It is then clear that AGB estimates produced by BIOMASS would greatly benefit from the exploitation of ancillary information about how to fine-tune the retrieval algorithms. This information is foreseen to be collected during an initial calibration and validation (Cal-Val) phase of the mission, where the produced biomass maps will be validated against ground measurements. A key role in the Cal-Val strategy will be played by the analysis and evaluation of data collected during an initial phase where system's orbit will be adjusted to gather multiple acquisitions over the same sites, characterized by small baselines and a repeat pass time on the order of a few days, thus allowing a nonmodel-based reconstruction of the forest vertical structure through SAR tomography (TomoSAR) [6], [11], [20]–[22]. This phase, hereafter referred to as the tomographic phase, will cover 10%–15% of the world's forest biomes, and is expected to provide useful insights for improving forest height and AGB retrieval during the rest of mission lifetime.

The employment of TomoSAR to investigate the vertical structure of forested areas has been addressed in several papers in past years, producing results that support the added value of this technique for remote sensing of forested areas. In particular, we deem it relevant to recall here the following results as shown below.

1) At P-band, significant backscattered power contributions are observed to come from the ground level, not only in co-polarized channels but in cross-polarized channels as well; this indicates that double-bounce contributions from trunk–ground and canopy–ground contributions are not negligible at this frequency band [19], [20].
2) Both forest height and terrain topography can be accurately estimated based on tomographic data [20], [23].

Still, one important factor is missing, i.e., the understanding of the link between AGB and tomographic measurements. The aim of this paper is to fill this gap. In order to do this, we present a TomoSAR analysis of the tropical forest site of Paracou, French Guiana, study the correlation between *in situ* AGB measurements and backscattered power at different heights within the vegetation, and provide an interpretation of the results. The analysis is based on the dataset collected by Office National d'Études et de Recherches Aérospatiales (ONERA) in 2009 in the frame of the ESA TropiSAR campaign [24].

The paper is organized as follows: Section II presents the SAR tomography methodology. In Section III, the study site is introduced, and in Section IV the P-band SAR tomography results are shown. In Section V, the relationship between radar measurements and AGB is evaluated, and the inversion results are presented. Section VI gives the interpretation of the results, and Section VII provides the discussion and finally the conclusions.

II. TomoSAR: Basic Concepts and Processing Chain

Tomographic processing allows the conversion of the multibaseline stack of SAR images into a multilayer stack of SAR images, where each image represents the complex reflectivity associated with a layer at a certain height above the ground. The basic principle of tomographic processing can be stated in relatively simple terms as follows. We consider a multibaseline dataset of single look complex (SLC) SAR images acquired by flying the sensor along N parallel tracks, and let $y_n(r, x)$ denote the complex-valued pixel at slant range, azimuth location (r, x) in the nth image. Assuming that each image within the data stack has been resampled on a common master grid, and that phase terms due to platform motion and terrain topography have been compensated for, the following model holds [21], [22], [25]:

$$y_n(r, x) = \int S(\xi, r, x) \exp\left(j \frac{4\pi}{\lambda r} b_n \xi\right) d\xi \tag{1}$$

where b_n is the normal baseline relative to the nth image with respect to a common master image; λ is the carrier wavelength; ξ is the cross-range coordinate, defined by the direction orthogonal to the radar line of sight (LOS) and the platform track; $S(\xi, r, x)$ is the average scene complex reflectivity within the slant range, azimuth, and cross-range resolution cell [22]. In (1) states that SAR multibaseline data and the cross-range distribution of the scene reflectivity constitute a Fourier pair. Hence, the latter can be retrieved by taking the Fourier transform of the data along the baseline direction. The final conversion from cross-range to height is then obtained through straightforward geometrical arguments. The resulting vertical resolution is approximately [21]

$$\Delta z \simeq \frac{\lambda}{2} \frac{r \sin\theta}{b_{\max}} \tag{2}$$

where θ is the radar look angle and $b_{\max}$ the overall normal baseline span. Equation (2) defines the so-called Rayleigh limit, well known in the field of array processing and tomography. The other equation that rules the design of a TomoSAR campaign is the one relative to the height of ambiguity, i.e., the maximum forest height that allows unambiguous vertical imaging [25]. This is easily obtained as

$$z_a \simeq \frac{\lambda}{2} \frac{r \sin\theta}{b_{\min}} \tag{3}$$

where $b_{\min}$ is the minimum baseline between any two acquisitions. The condition to ensure correct tomographic imaging

[2]Single baseline PolInSAR height estimation is usually carried out by exploiting prior assumptions about ground contributions, which however can strongly vary depending on local slopes [6], [20].

is to let the height of ambiguity exceed the forest height, i.e., $z_a > h$, where h is forest height. Assuming N equispaced passes and letting $z_a = \beta h$ (with $\beta > 1$), we get

$$\Delta z \simeq \beta \frac{h}{N}. \tag{4}$$

For example, by letting $\beta = 2$, which is a safe condition to ensure unambiguous imaging, we get that the forest volume can be split into $N/2$ independent layers.

A common issue of SAR tomographic surveys is that the resolution allowed by the Rayleigh limit is often too coarse when compared to the vertical extent of the observed scene, and the hypothesis of equispaced baselines often breaks down in case of airborne campaigns. For this reason, tomographic processing is usually carried out by sophisticated spectral estimation techniques that provide super-resolution imaging and counteract the effects of irregular baseline sampling. For a comprehensive discussion of these methods, the reader is referred to the excellent works in [26] and [27].

Still, although such techniques allow the recovery of details not accessible otherwise, they result in poor radiometric accuracy in the case of distributed targets, which limits their application to the aim of yielding quantitative measurements in a completely model-free fashion. This task, however, becomes possible whenever the available baseline set allows it, resulting in the possibility to carry out model-free unbiased measurements of the vertical distribution of the backscattered power. This is the case of the P-band dataset analyzed in this paper, as will be discussed in the following. For this reason, the image formation along the vertical direction has been carried out in this paper simply by coherent focusing, i.e., by Fourier-transforming the data with respect to the normal baseline. This way of processing does not optimize vertical resolution. Yet, it yields radiometric accuracy along the vertical direction.

Prior to applying the simple approach described above, it is usually necessary to take a number of factors into account. In the first place, blurring, which affects the quality of tomographic focusing, can arise as a result of: 1) phase disturbances resulting from uncompensated platform motion [28], [29], and 2) irregular baselines sampling, the effective baseline set being determined by the actual trajectories along which the sensor has been flown. These two factors need to be carefully taken care of to provide accurate measurements of the vertical distribution of the backscattered power. Terrain topography has to be considered as well, as it plays a threefold role in tomographic measurements. First, in tomographic analyses of forested areas, the interest is in the vertical backscattered power distribution within the vegetation layer. Accordingly, terrain topography has to be removed, in such a way as to reference each image within the multilayer stack produced by the tomographic processing to a certain height above the ground, rather than to a height with respect to a fixed reference. Furthermore, topography determines a variation of the backscattered power that is not correlated to vegetation, and thus it may produce a significant bias in the backscattered power [16]. Finally, knowledge of terrain topography is required in order to analyze the *in situ* data. The implemented processing chain is depicted in Fig. 1. A description of each block is provided in the following sections.

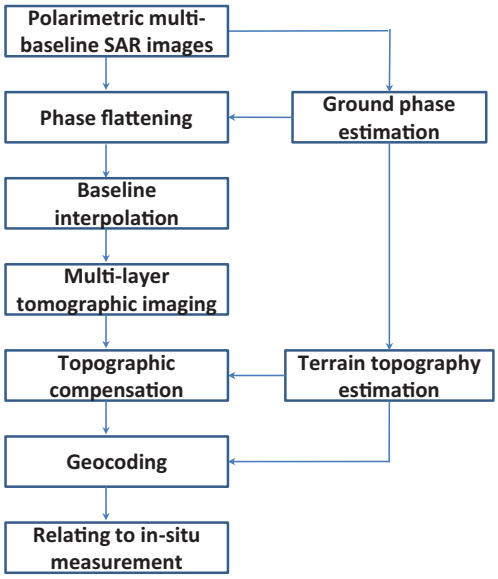

Fig. 1. Proposed SAR tomography processing chain.

A. Phase Calibration, Baseline Interpolation, and Tomographic Imaging

A complete procedure for phase-calibrating the data stack and resampling the multibaseline array on a regular grid was already discussed and validated against the same dataset analyzed in this paper in [19], which the reader is referred to for details. The procedure is then just briefly recalled here for sake of completeness.

Phase calibration was carried out according to the two-step procedure proposed in [29] and [30]. In the first step, the algebraic synthesis technique is used to recover the matrix of interferometric coherences associated with ground-only contributions [31]. In the second step, the phase-linking algorithm is used to retrieve the best estimate of the ground phases [32]. Phase calibration is then performed by removing the retrieved ground phases from the SLC data stack, which corresponds to the block referred to as phase flattening in Fig. 1. It is important to note that the retrieved ground phases are directly related to the optical paths from the ground layer to the N sensors, and are therefore determined not only by the terrain topography but also by the phase disturbances deriving from platform motion. Accordingly, removing the ground phases brings two advantages. The first is the removal of the propagation disturbances, which allows correct focusing along the vertical direction. The second is the removal of terrain topography, resulting in the contributions from the terrain to be automatically focused at 0 m, independently of the actual topography.

Vertical focusing from irregularly sampled data is a well-known problem in the literature on SAR tomography, resulting in several approaches for its treatment [26], [28]. In this paper, a simple yet quite fast and robust solution is given. In order to simulate a null displacement from the ideal regularly spaced trajectories, the image stack has been interpolated at each slant range azimuth location on a regularly sampled baseline grid [19]. The interpolator has been implemented by employing a linear kernel, which is properly adjusted in phase so as to guarantee the maximal flat response between 0 and 40 m, consistent with the vertical extent of the vegetation

layer [19]. Based on numerical simulations, the residual error with respect to the ideal case of regularly sampled baselines has been assessed to be less than 0.2 dB over the whole imaged scene.

After phase calibration and baseline interpolation have been carried out, tomographic imaging has been performed simply by taking the Fourier transform (with respect to the normal baseline) of the multibaseline SLC dataset at every slant range, azimuth location. The result of this operation is a multilayer SLC set, where each layer is referred to a fixed height above the terrain. We will hereafter refer to each image within the multilayer data stack simply by the associated height (i.e., 10-m layer, 20-m layer, etc.), or as ground layer for the image focused at 0 m.

B. Terrain Topography Estimation

Knowledge of terrain topography is required for compensating the backscattered power measurements for the local terrain slope, as well as for mapping the multilayer data stack onto ground geometry. In this paper, terrain topography has been obtained by analyzing the ground phases, which are available as a by-product of the phase calibration procedure described in Section II-A. In detail, neglecting estimation noise, the retrieved ground phase in the nth image can be expressed as the sum of two contributions: one relative to the topography, and the other to propagation disturbances. That is

$$\varphi_n = \frac{4\pi}{\lambda r \sin\theta} b_n z_g + \eta_n \tag{5}$$

where z_g is the local terrain height and η_n is the phase disturbance in the nth image. Terrain height can then be retrieved at each slant range, azimuth location by linear fitting the (unwrapped) ground phases in (5) with respect to the normal baseline, as is customary in multibaseline InSAR, see, e.g., [33]. Of course, the presence of phase disturbances results in a residual error in the terrain height. Such an error impacts mostly on the lowest spatial frequencies of the retrieved terrain height, due to the fact that the phase disturbances exhibit a low-pass behavior. Accordingly, the residual error can be corrected by imposing further constraints on the low-frequency components of terrain topography, which are easily derived from the available digital elevation models (DEMs) [23]. The approach followed in this paper is the one given in [23], which provides a formal algebraic framework for imposing external constraints. A DEM of the area from the Shuttle Radar Topographic Mission (SRTM) [34] has been used to derive the mean topographic slopes along azimuth and range, which have been employed to constrain topography retrieval. A comparison with the available analysis of LiDAR DEM has shown no significant bias greater than 4 m and standard deviation less than 3 m.

C. Topographic Compensation

As outlined above, topographic slope determines a variation of the backscattered power that is not related to vegetation [16], and thus it has to be properly compensated for in order to relate backscatter measurements to AGB. Let $S(z, r, x)$ denote a complex-valued pixel from the image corresponding to the layer at height z within the multilayer data stack produced by the tomography processing. The topographic compensation has been performed as in [35]

$$P(z, r, x) = |S(z, r, x)|^2 \cdot \sin(\theta - \alpha) \tag{6}$$

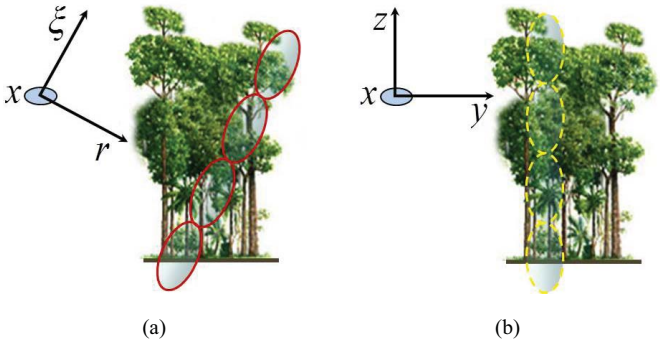

Fig. 2. (a) Forest tomographic resolution cells in slant range (radar) geometry. (b) Forest tomographic resolution cells in ground range geometry.

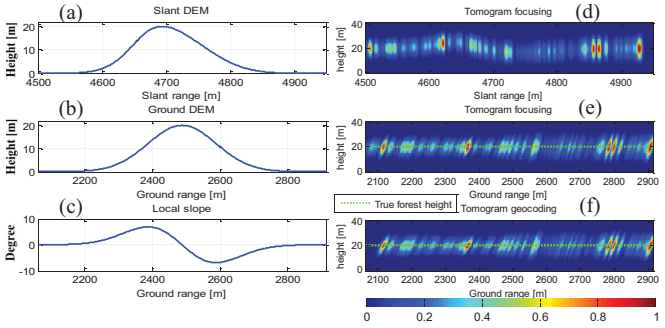

Fig. 3. (a) Simulated DEM in slant range coordinate. (b) Ground range coordinate. (c) Corresponding local slope in ground range coordinate. (d) Tomogram focused in radar geometry. (e) Tomogram focused in ground geometry. (f) Geocoded tomogram.

where $P(z, r, x)$ is the signal backscattered power, α is the local ground slope, and θ is the radar look angle. In general, it would be preferable to normalize the layers differently, as will be discussed in Section IV-B.

D. Geocoding

Being able to link precisely one pixel in the slant range geometry image to the pixel in ground range geometry is essential, especially for studying the relationship between SAR and *in situ* measurements. Once the vertical distribution of the backscattered power has been retrieved in radar geometry, an interpolation step is required in order to convert to ground geometry. The difference of these geometries is depicted in Fig. 2.

This operation is conceptually not different from the standard geocoding of SAR images [36], with the only exception that the elevation location of the targets has to be accounted for, resulting in an increase of dimensionality in the interpolation step. Accordingly, the correct implementation of such an interpolation step requires the knowledge of terrain topography, analogous to conventional geocoding.

To illustrate the result of this processing step, we simulate tomograms from a forest scene over a terrain with a given DEM. The simulated system geometry is the same as the actual TropiSAR dataset. The simulated scene consists of a single phase center representing the tree tops, placed at a constant height of 20 m above the ground from near to far range. The left panel of Fig. 3 shows the simulated DEM in (a) (radar) slant range geometry, (b) ground range geometry, and (c) the corresponding local slope. The top-right and

middle-right panels of the same figure report the outcome of the tomographic processing as performed in (d) slant range geometry or (e) directly in ground geometry. In both cases, the tomogram has been flattened by removing the ground phase in such a way that the terrain always corresponds to 0 m. The undulation visible in the slant range tomogram (d) is due to the bias about target height induced by local slope [37]. This phenomenon is no longer present in the ground geometry (e), which was focused while accounting for terrain topography. Finally, we report in the bottom right panel of Fig. 3(f) the ground geometry tomogram obtained by geocoding the one focused in radar geometry. It is worth remarking that, except for a few samples at the boundaries, the tomograms in panels (e) and (f) are identical, indicating the validity of the implemented geocoding procedure.

III. TropiSAR Paracou Datasets

The TropiSAR campaign was conducted in French Guiana in the summer of 2009 in the framework of the Phase A studies pertaining to the BIOMASS mission [4], [6]. The main campaign objectives were the evaluation of P-band radar imaging over tropical forests for AGB and forest height estimation [38]. Two main forest sites have been studied: Nouragues and Paracou. For both, an extensive *in situ* database was available. Seven SAR flights were conducted with the SETHI system from ONERA both at P-band and L-band, a number of which were suitable for tomographic processing. The dataset analyzed in this paper is the P-band data related to the Paracou test site.

A. Paracou Test Site

The Paracou experimental site is located in a lowland tropical rain forest near Sinnamary, French Guiana (5° 18' N, 52° 55' W) [39]. The elevation is between 5 and 50 m, and mean annual temperature is 26 °C, with an annual range of 1 °C–1.5 °C. Rainfall averages 2980 mm yr^{-1} (30-year period) with a three-month dry season (<100 mm $month^{-1}$) from mid-August to mid-November [40]. The landscape is characterized by a patchwork of hills (100–300-m wide and 20–35-m high) separated by narrow streams. The forest in Paracou is classified as a lowland moist forest with 140–200 species per hectare, as specified in the forest census of all trees with diameter at breast height (DBH) > 10 cm.

To analyze the relationship between tomographic data and AGB, we use the *in situ* forest measurements on 16 permanent plots established starting from 1984 in the Paracou primary forest. These are 15 plots of 250 × 250 m^2 (6.25 ha) each and one plot of 500 × 500 m^2 (25 ha) in which all stems of DBH ≥ 10 cm have been mapped and regularly surveyed since 1986. For the Paracou primary forests, the number of trees with DBH > 10 cm ranges between 400 and 700 stems per hectare.

From 1986 to 1988, nine of these fifteen 6.25-ha plots underwent three different logging treatments ranging from mild to severe for a study of the forest responses to logging intensities. In Treatment 1, selected timbers were extracted, with an average of ten trees of 50 or 60 cm DBH removed per hectare. Treatment 2 was logged as in Treatment 1, followed by timber stand improvement by poison-girdling of selected noncommercial species, with about 30 trees of 40 cm DBH removed per hectare. Treatment 3 was logged as in Treatment 2 for an expanded list of commercial species, with about 45 trees of 40 cm DBH removed per hectare. In 2009, the degraded plots had the AGB at 1-ha resolution ranging between 250 and 392 t ha^{-1}, depending on the initial logging intensity [24].

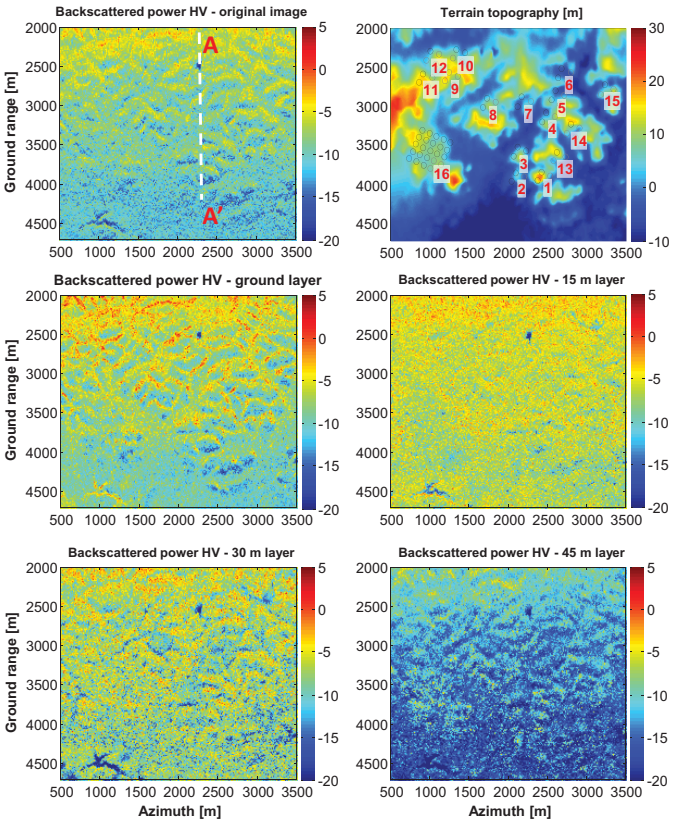

Fig. 4. Tomographic results over the Paracou study site. HV backscattered power for four tomographic layers associated with four different heights above the ground 0 (ground layer), 15, 30, and 45 m. The top left panel presents the original HV image. The top right panel is the terrain topography with circles relative to center areas where *in situ* AGB measurements are available.

B. SAR Datasets

The SAR system used in the TropiSAR campaign is the ONERA airborne system SETHI [24]. The P-band SAR has a bandwidth of 335–460 MHz and the resolution is about 1 m in slant range and 1.245 m in azimuth direction [38]. The whole TropiSAR datasets including *in situ* data are available through the archive of the ESA. Details on access to campaign data can be found at the ESA EOPI portal (http://eopi.esa.int), under the campaigns link.

In this paper, we use the Paracou tomographic dataset, which consists of six fully polarimetric SLC images at P-band acquired on August 24, 2009. The baselines have been spaced vertically with a spacing of about 15 m. The trajectory flown is lower than the reference line (3962 m) with a vertical shift of 15, 30, 45, 60, and 75 m, respectively.

Since the tomographic flight lines are in a vertical plane rather than in a horizontal plane, the phase-to-height factor has a small variation across the scene swath, and similarly for the height of ambiguity (ranging between 102 and 185 m) well above the vegetation height [38]. The resulting Fourier vertical resolution is about 20 m (±10 m at −3.5 dB), whereas forest height ranges from 20 m to over 40 m. These features make it possible to map the 3-D distribution of the scene complex

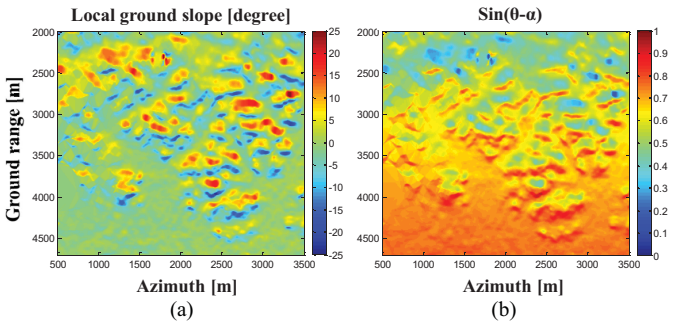

Fig. 5. (a) Local ground slope. (b) Factor $\sin(\theta - \alpha)$.

reflectivity by coherent focusing, i.e., without assuming any physical model or employing super-resolution techniques.

C. AGB Datasets

The AGB data were estimated based on forestry censuses, making use of allometric equations to convert the measured dimensions (DBH, total tree height and wood density) into AGB for each tree. As stated above, within the 16 experimental plots, all individual trees with a diameter >10 cm have been measured. In order to increase the number of plots for statistical analysis of the relationships between biomass and backscattered power, the plots have been subdivided into subplots. In this paper, plots 1–15 are subdivided into four subplots of 125×125 m^2 (1.5 ha), while plot 16 is divided into 25 subplots of 100×100 m^2 (1 ha), resulting in 85 independent subplots for which the AGB data are reconstructed (see top right panel in Fig. 4). The size of the plots of 1 and 1.5 ha was chosen for reducing speckle effect and uncertainties in *in situ* AGB estimates ($< 9\%$ at 1 ha [41]). For the 85 plots, the mean AGB ranges from 250 to 450 t ha^{-1}, and the tree top height varies from 20 to 40 m with the average value being about 28 m.

IV. Results From Tomography

Tomographic focusing has been carried out for all polarizations according to the processing chain discussed in Section II, resulting in three (HH, HV, VV) multilayer SLC data stacks. We recall that we refer to each image within a multilayer data stack simply by the associated height (i.e., 10-m layer, 20-m layer, etc.), or as ground layer for the image focused at 0 m. It is also worth remarking that the implemented phase calibration procedure automatically steers ground contributions at 0 m, so that the height of each layer is always to be intended as being relative to terrain elevation.

A. Multilayer Images

First of all, to clarify how the terrain topographic contribution can be handled by SAR tomography, we do not include the topographic compensation step (see Section II-C) in the processing chain. Fig. 4 shows the HV backscattered power for layers at 0 (ground layer), 15, 30, and 45 m. The backscattered power relative to one image from the original multibaseline data stack (i.e., nontomographic) is shown in the top left panel of Fig. 4 to provide a comparison, and the terrain topography is shown in the top right panel. The information on slope variation and the factor $\sin(\theta - \alpha)$ are provided in Fig. 5.

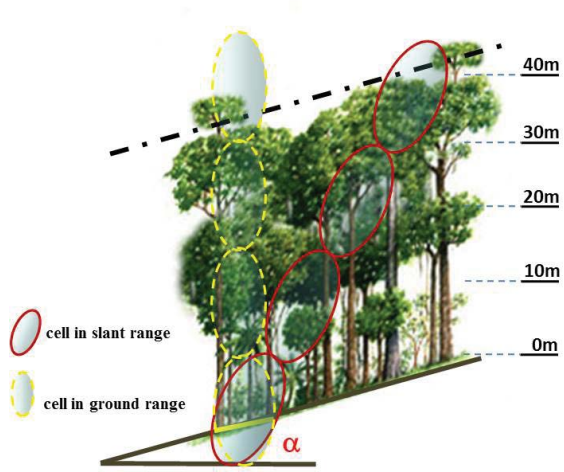

Fig. 6. Schematic view of the tomographic resolution cells in a forest located on a terrain slope. This illustration depicts an interpretation the high correlation between the backscattered power of the outermost cell and the ground topography slope. It can be observed that the intermediary cells are always filled up by trunk and woody branches irrespective of the slope.

The four tomographic layers are observed to be different in their information content. In particular, the ground and the top (45 m) layers show strong topographic effect, whereas the middle layer images appear much less affected by topography. This phenomenon may be easily interpreted by taking a closer look at the distribution of the scatterers within the tomographic resolution cell in both geometries of slant and ground range, see Fig. 6.

In the bottom resolution cell, the tomographic layer SAR signal is affected by terrain slope the same way as in traditional SAR images of bare surfaces with slope. In the resolution cell corresponding to tree top height, the signal can also be affected by topography, although more weakly, because in general the top height of natural forests follows terrain slope. Finally, cells inside the canopy are always filled up by trunk and woody branches irrespective of the ground slope, resulting in the topographic slope to have a minor effect on signal power.

B. Topographic Compensation

Based on the interpretation of the previous section, it is possible to classify the tomographic layers as surface layers, i.e., the ground (0 m) and the topmost layers, and volume layers, i.e., the middle height ones. In order to relate the tomographic data to *in situ* measurements, such as AGB, it is required that the backscattered power is normalized with respect to a surface for surface layers and to a volume for volume layers. We propose to use a geometric projection law [35], for the normalization both of surface and volume layers. The results are reported in Fig. 7. From the left panels in Fig. 7, it is possible, in some cases, to observe a reduction of the nonnormalized backscattered power with increasing look angle. The surface layers, namely the ground and the top layer (45 m), show the trend visibly, whereas the middle layers look less sensitive. The right panels in Fig. 7 show the backscattered power normalized by the factor $\sin(\theta - \alpha)$. We note that the change of the backscattered power from near to far range is reduced for the surface layers. For the middle (volume) layers, a normalization with respect to the volume size would be

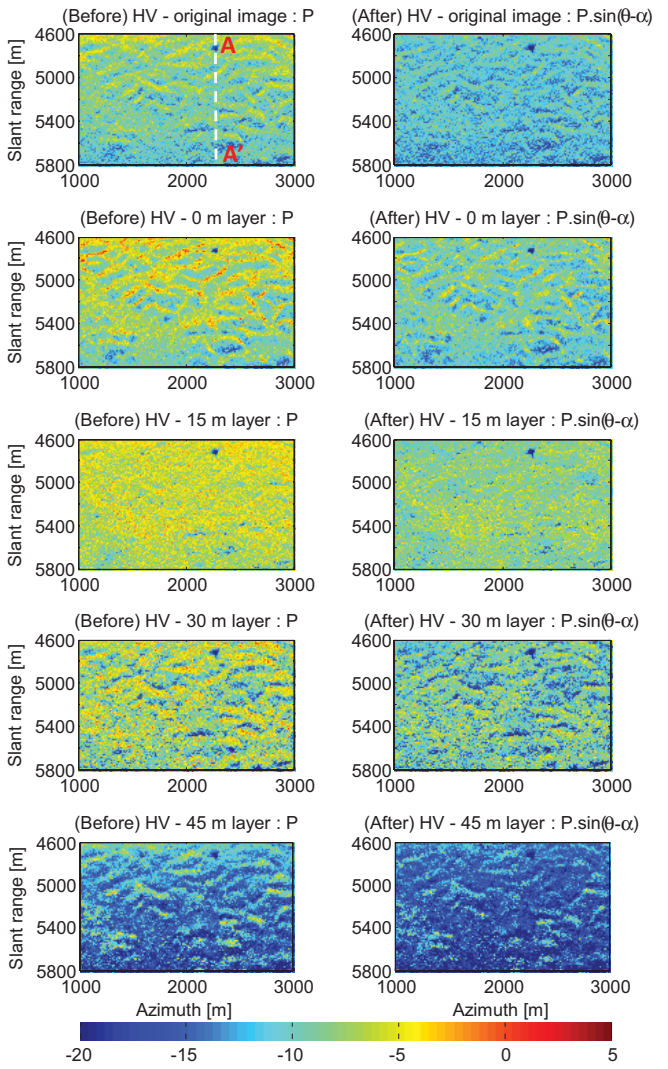

Fig. 7. Left panels: Before topographic compensation. Right panels: After topographic compensation. HV backscattered power for four tomographic layers associated with four different heights above the ground 0 (ground layer), 15, 30, and 45 m. The two top panels present the original HV image.

preferable. However, the TropiSAR data analyzed in this paper are characterized by a small variation with range of the vertical resolution, while slant range and azimuth resolution are constant. So, this last normalization has not been carried out.

C. Tomographic Profiles

A convenient way to observe the forest vertical structure at a local scale is provided by taking a tomographic profile, namely a slice of the multilayer data stack corresponding to a constant ground range or azimuth value. Fig. 8 presents the tomographic profile of a constant azimuth section AA' (x = 2270 m, see Fig. 7) at HH, HV, and VV. All panels have been normalized in such a way that the sum along height is unity, in order to help visualization. The white line denotes forest top height derived from LIDAR measurements.

The first observation is that for all polarizations the total backscattered power results from the interaction with all layers, including the ground layer. The contribution of the vegetation is important. Yet, relevant contributions from the ground level beneath the forest are observed. In HH and VV,

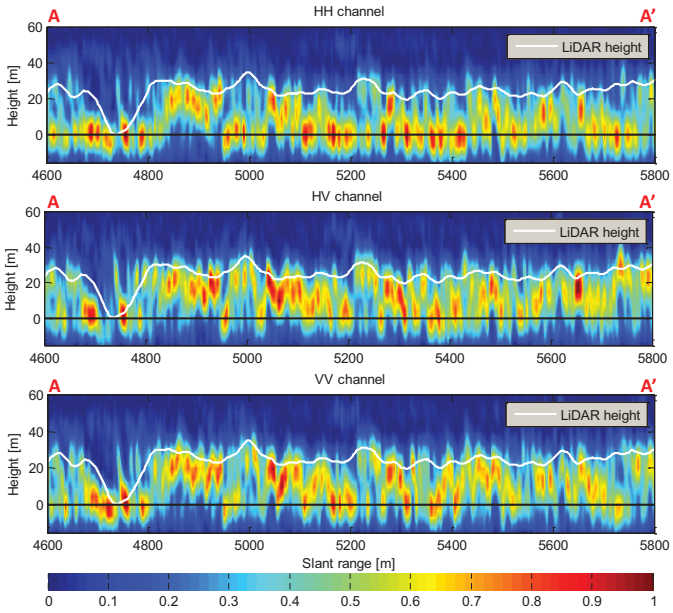

Fig. 8. Tomographic reconstruction along the same azimuth cut AA' (see Figs. 4 and 7) in all polarizations, from top to bottom: HH, HV, and VV. The while line denotes the LIDAR height measurements. All panels have been normalized in such a way that the sum along height is unity.

the ground contribution is more important than the contribution of the vegetation layers, indicating double-bounce scattering from either trunk–ground or branch–ground interactions dominating volume scattering. In HV, instead, the contribution of the ground layer appears to be less important than that of the vegetation layers. These results show that the scattering mechanisms in tropical forest are quite different from boreal forests where the dominating contribution was observed to be associated with the ground level in all polarizations [20], [42]. Finally, it is worth noting that the spatial distribution of the backscatter over the analyzed transect in the upper layers (20–40 m) is quite similar in all polarizations.

V. Relation to Forest Biomass

A. Linear Regression

Prior to analyzing the correlation, it is worth remarking that it is necessary to take the topographic compensation procedure (see Section II-C) into account. To appreciate the effectiveness of this step, we report here both the results of: 1) no topographic compensation, and 2) topographic compensation. In Fig. 9, topographic compensation results are shown. These figures display the backscattered power in HV and HH of the 85 plots as a function of *in situ* AGB, for nine layers varying from 0 to 40 m, at 5-m interval. As observed in Section IV-A, layers corresponding to different heights provide different information content, so that correlation of backscatter power with AGB is also expected to differ among layers. These graphs indicate that linear regression can be used to quantify the relationship between the backscattered power and AGB. A linear fit has then been performed by assuming a classical log law [7]

$$B = a \cdot \log 10(P) + b \tag{7}$$

where B is the AGB; P is the backscattered power; and a and b are factors defining a linear trend. The quality of the linear fit is assessed using the Pearson linear correlation r_P [43],

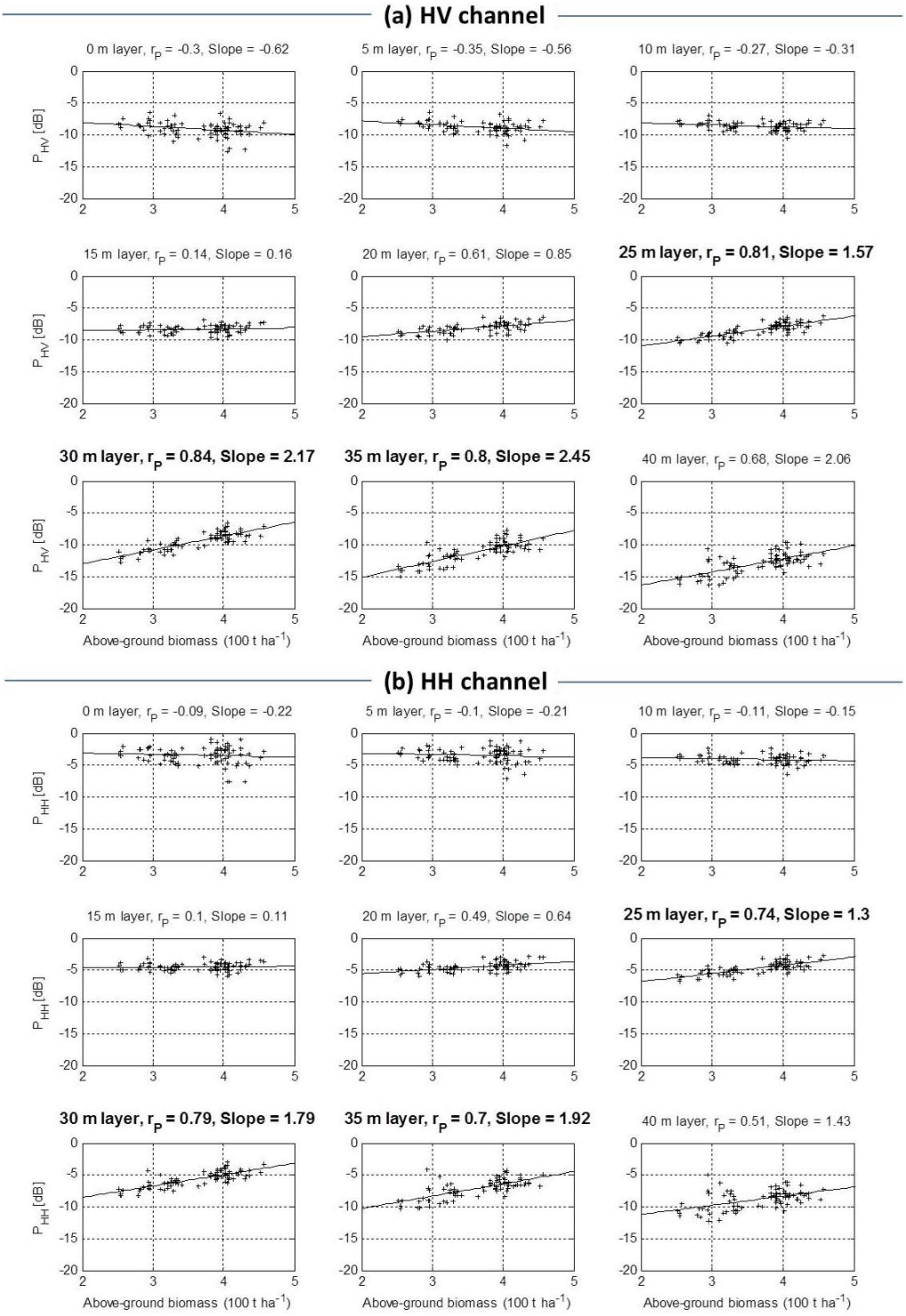

Fig. 9. Sensitivity of backscattered power at different layers to AGB. (a) HV channel. (b) HH channel. r_P is the Pearson correlation coefficient. Slope is referred to the angular coefficient of the resulting linear fit.

which measures the degree of association between the *in situ* AGB and backscattered power. The full sets of 85 plots is considered, for which the significance level for the Pearson correlation at 1% and 5% risk is respectively about 0.27 and 0.21 [43].

Although there is no topographic compensation in the data, we find that the upper layers (i.e., 30 and 35 m) have strong correlation with the AGB.[3] The correlation is further improved by normalizing the backscattered power by the factor $\sin(\theta - \alpha)$. Fig. 9 reports this result. Applying the topographic compensation, the dispersion is reduced in all layers, and the

[3]The correlation values in HV channel at 30- and 35-m layer are 0.70 and 0.64, respectively.

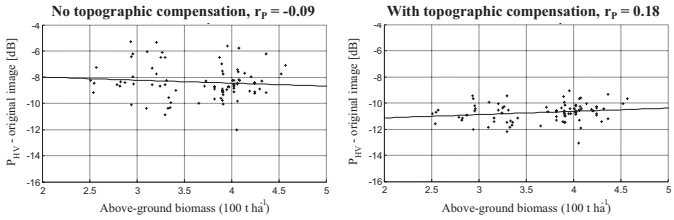

Fig. 10. Left panel: Sensitivity of the HV backscattered power of the original (nontomographic) data to AGB without topographic compensation. Right panel: Same with topographic compensation. r_P is the Pearson correlation coefficient. Slope is referred to the angular coefficient of the resulting linear fit.

correlation of upper layers with biomass is enhanced from $r_P = 0.7$ to $r_P = 0.84$ in HV 30-m layer.

The following interpretation focuses on the results after proper topographic compensation. The best correlation ($r_P = 0.84$) is found for the 30-m layer in HV, for which the backscattered power increases by about 4.3 dB as AGB changes from 250 to 450 t ha^{-1} (about 1.1 dB for 50 t ha^{-1}). For the 35-m layer, the backscatter dynamic range is larger, but the correlation is reduced and the dispersion is increased. For the 40-m layer, the correlation decreases and the dispersion increases despite having the same dynamic range as the 30-m layer. These analysis results are in agreement with the observations in Section IV-A. It is worth noting that the 30-m layer exhibits a noticeable correlation with AGB not only in HV but also in HH and VV,[4] indicating that the co-polar channels may be used as well for AGB estimation. This is consistent with the tomographic profiles discussed in Section IV, whose spatial distribution was observed to show poor sensitivity to polarization in the upper layers.

In order to provide a comparison, the same sensitivity analysis has been carried out considering the backscattered power of the original (i.e., nontomographic) data. Results are reported in Fig. 10. It can be immediately seen that nontomographic data exhibit a much lower sensitivity to AGB than tomographic data, resulting in the Pearson linear correlation to drop from $r_P = 0.84$ to $r_P = 0.18$ (see right panel of Fig. 10). This low sensitivity to AGB of the backscattered power for high biomass values requires more elaborate topographic correction as well as development of a suitable biomass indicator from POLSAR intensity for AGB retrieval. However, even using the elaborate POLSAR method, r_P increases to 0.63 [6], which is far below the TomoSAR results.

B. Biomass Inversion

Based on the results and the discussion above, in this section an estimator is introduced to retrieve the AGB based on the backscattered power in HV for the 30-m layer. AGB estimation is carried out according to the log-linear law expressed in (7). The estimator parameters have been set by using ten training samples out of 85 plots. The retrieved AGB values are then validated with the remaining 75 samples. Performance is assessed by evaluating the root-mean-square error (RMSE) between *in situ* measurements and the estimated AGB values. Results are reported in Fig. 11. The Pearson correlation is found to be $r_P = 0.84$, whereas the RMSE turned out to be lower than 10%.

[4]VV results are not shown here because of this similarity.

VI. Interpretation

Based on the results shown in the previous section, we deem there are two findings that need be highlighted.

1) The ground layer is poorly or negatively correlated to AGB and strongly varies with topographic slopes.
2) The 30-m layer is significantly correlated to AGB.

The aim of this section is to provide an interpretation of the results highlighted above. In order to do this, it is first require a brief discussion about the physics of radar scattering from forested areas, in order to recall what the expected properties are of TomoSAR imaging of forested areas. As shown in many works in the literature, forested areas can be characterized as the ensemble over the ground of trunks and crown, to be described as a volume of random scatterers representing leaves and branches [44]–[48]. According to this general model, the interaction of radar waves with a forest can be described by modeling the ground as a half-space dielectric and using image theory [44], [49], [50]. Four scattering mechanisms result [44], [49]: ground backscattering; double bounce scattering from ground–trunk and vegetation–ground interactions; volume scattering; and multiple scattering (triple and more bounces) interactions. Ground backscattering is clearly associated with the ground level. As such, these contributions are captured in TomoSAR imaging by the ground layer. Concerning double-bounce contributions from ground–trunk and vegetation–ground interactions, through simple geometric arguments and assuming flat terrain, it is possible to see that the distance covered by the wave as it undergoes the two consecutive specular reflections on the ground and on the target, or vice versa, is equal to the distance between the sensor and the projection of the target onto the ground [22]. It follows that, under the assumption of a flat terrain, every double-bounce mechanism is located at the ground level. Accordingly, it will be captured in TomoSAR imaging by the ground layer. However, this conclusion does not hold in sloping areas, in which case the contributions of double bounces rapidly vanish as terrain slope increases [16], [19], [44], [49]. In particular, in [19], which is specific to the test site analyzed in this paper, it was found that trunk–ground contributions vanish as the terrain slope approaches 6°. Concerning third-order scattering (triple bounces), it makes sense to retain that ground-to-target-to-ground contributions may be neglected, by virtue of the higher attenuation, with respect to the double-bounce case, undergone by the wave in further reflection on the ground and in the subsequent propagation through the trunk layer and the canopy layer of adjacent trees. Accordingly, higher order multiple scattering can be neglected as well. Vegetation backscattering is then the sole scattering mechanism that can give rise to backscattered power contributions from above the ground. As such, it is captured in TomoSAR imaging by layers focused above the ground. Based on this simple, yet largely retained, model, we will assume in the following that: 1) the ground layer captures backscattering contributions from the soil and from lower vegetation, and double bounce contributions from trunk–ground and vegetation–ground double bounce interactions, and 2) each layer above the ground captures backscattering contributions associated only with the portion of vegetation at the layer height. It is also important to note that no action is taken by the TomoSAR processor to compensate for wave extinction. This means that the backscattered power level sensed in each layer is sensitive to the forest density in the layer above, which is particularly important when considering

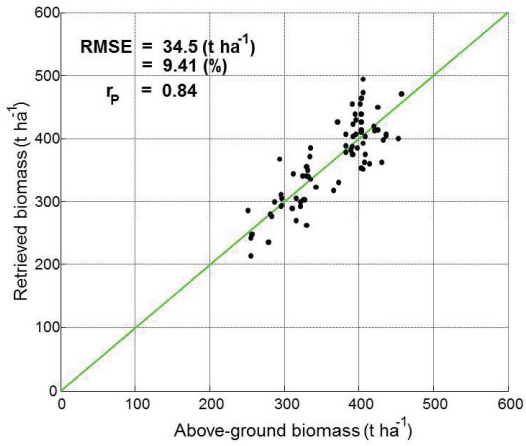

Fig. 11. Comparison between *in situ* AGB and AGB derived from inversion of the P-band HV 30-m layer. The RMSE in retrieved AGB is about 9.4%, indicating the very good performance for the AGB estimation from tomography data from this high range of tropical forest biomass.

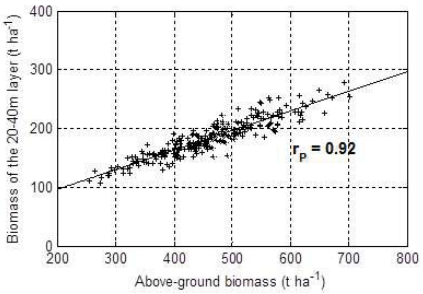

Fig. 12. Correlation between the proportion of biomass contained in the 20–40-m layer and the total AGB using the TROLL model. The linear relationship can be established, as confirmed by a 0.92 correlation coefficient.

the ground layer. With this in mind, we suggest the following interpretation for the results.

For the layers below 20 m, the correlation between the backscattered power and AGB is very weak (and with negative trend, especially for HV). This can be explained by the following: 1) the trend is negative because of extinction, in that the higher the trees, the weaker the signal penetrating down to the ground, and 2) the scatter plots are dispersed since the dominant scattering mechanisms may change drastically when the ground surface is tilted relative to the horizontal.

For layers between 20 and 40 m, the correlation between backscatter and AGB becomes highly significant, implying that 1) the perturbing effect of the ground contribution is minimized (i.e., TomoSAR focusing allows a very good rejection of ground contributions), and 2) there is a strong correlation between the biomass contained in this layer and the total AGB.

To evaluate the correlation between biomass within the 20–40-m layer and the total AGB, Monte Carlo simulations have been performed based on the TROLL model [51], which is a spatially explicit forest growth model designed to study structural, successional, and spatial patterns in natural forests with special emphasis on neotropical rainforests as in French Guiana. In this model, because of the large number of species in the forest, they have been grouped into functional type groups (light demanding, shade-tolerant, and intermediary), and into four height classes (0–5, 6–15, 15–25, and 25–50 m). The parameters of the model for each of the species groups have been determined using field data in French Guiana. For our simulations, three classes of DBH have been considered with their corresponding number of trees per hectare [51]. A Gaussian dispersion around these mean DBH is then governed by the Monte Carlo process, from which the other characteristics (total height and crowns shape) are deduced using the TROLL tree architecture allometry. Considering a surface extent of 400×400 m^2 and 4 different random seeds for the Monte Carlo process, $8 \times 8 \times 4$ samples of 50 m^2 have been generated from which the biomass between 20 and 40 m can be extracted from the total AGB. Fig. 12 shows the model-derived proportion of biomass contained in the 20–40-m layer in the total AGB. The simulation result shows that, for the tropical forest, there is a strong relationship ($r_P = 0.92$) between the biomass within the 20–40-m canopy volume and the total AGB.

VII. Conclusion

As stated in the BIOMASS Report for Selection issued in May 2012 [6], the role of tomography within the BIOMASS Mission is to provide new insights into the interactions of P-band waves with the forest structure, resulting in inputs to be used to improve forest height and AGB estimation for the rest of Mission lifetime. As seen from Section VI, we have gained understanding on the scattering mechanisms of a tropical forest with high biomass values and located over a terrain with topography. We have also demonstrated how tomography is related to forest biomass.

1) Contributions from the ground level are poorly or negatively correlated to AGB and strongly vary with topographic slopes.
2) The 30-m layer is significantly correlated to AGB. Similar features are encountered in all three polarizations.

To produce these results, a very simple approach was used, consisting in evaluating the correlation between AGB and backscattered power at different heights. Comparing the results against the correlation of the total (i.e., nontomographic) backscattered power for HV is the most straightforward way to demonstrate how useful the vertical resolution capabilities are.

The simplicity of this approach does not allow carrying out a fair comparison with PolSAR and PolInSAR methods. Results would be quite disappointing in the case where we implemented nontomographic estimation methods without tuning them for this dataset, as it is immediately understood by considering that the correlation to AGB is 0.18 for nontomographic data and 0.84 for tomographic data. On the other hand, nontomographic estimation methods can be properly tuned to adapt to the characteristics of the dataset, thereby greatly improving accuracy. A detailed comparison of different methods on the same dataset will be treated in future work.

Based on the result obtained, the TomoSAR method could be used to map AGB, in particular, for tropical forest where high accuracy in AGB is required to improve the carbon budget. However, the results obtained in this paper do not apply directly to a spaceborne system, as they were derived under different conditions (airborne and not spaceborne). Performance assessment for tomography in BIOMASS is currently an ongoing work. The analysis needs to account for: 1) ionospheric disturbances; 2) temporal decorrelation; 3) the 6-MHz bandwidth limit imposed by ITU regulations; 4) the role of the incidence angle (which cannot be mimicked with

airborne data along the whole swath); 5) environment effect such as rain; 6) the tradeoff between TomoSAR coverage and the frequency of global mapping; and 7) the limitation of the method in low biomass forests.

Concerning the 6-MHz bandwidth limit, TomoSAR imaging was shown to be feasible despite the 6-MHz bandwidth constraint imposed by ITU regulations for the BIOMASS system [6], [52], [53]. In [53], in particular, it was shown that the 6-MHz limit results in the vertical resolution to be lower bounded at about 15 m, which allows separation of up to 3–4 vertical layers in a mature tropical forest.

For TomoSAR coverage, because of its need for multibaseline, TomoSAR is planned to cover 10%–15% of the global forest coverage during the first phase of the mission. In this case, a strategy will be developed to use TomoSAR results as references to fine-tune PolSAR and PolInSAR. On the other hand, investigations are going on to assess the possibility to increase the TomoSAR coverage, with the possible expense on the mission lifetime.

To conclude, in this paper SAR tomography has been exploited for the retrieval of AGB in dense tropical forests based on TropiSAR 2009 datasets. The tomography methodology to derive the AGB information has been described. The processing chain for multilayer imaging, i.e., for deriving a synthetic image at a specific height above the ground, has been presented. Airborne SAR tomography, which allows accurate mapping of the vertical distribution of the backscattered power in each polarization, provides a new approach to understanding the scattering mechanisms at P-band in a tropical forest. Overall, TomoSAR appears now to be a novel tool to investigate AGB from radar measurements. The methodology and the results apply to the tropical forest, even over a terrain with topography.

Finally, despite the much work that remains to be done, SAR tomography at P-band appears a new way to have estimates and mapping of AGB, in particular in dense tropical forests.

ACKNOWLEDGMENT

The authors would like to thank the TropiSAR team for providing the TropiSAR datasets of excellent quality. They also would like to thank Dr. P. Dubois-Fernandez (ONERA), for the radar datasets which allowed them to do the tomographic processing along with the whole TropiSAR 2009 team, the Guyafor team and particularly Dr. L. Blanc for providing *in situ* data and LIDAR data used in this paper, and Prof. J. Chave and Dr. M. Réjou-Méchain for suggestions on biomass interpretation.

REFERENCES

[1] S. J. Wright, "Tropical forests in a changing environment," *TRENDS Ecol. Evol.*, vol. 20, no. 10, pp. 553–560, Oct. 2005.

[2] J. Tollefson, "Counting: Carbon in the Amazon," *Nature*, vol. 461, pp. 1048–1052, Oct. 2009.

[3] S. S. Saatchi, N. L. Harris, S. Brown, M. Lefsky, E. T. A. Mitchard, W. Salas, B. R. Zutta, W. Buermann, S. L. Lewis, S. Hagen, S. Petrova, L. White, M. Silman, and A. Morel, "Benchmark map of forest carbon stocks in tropical regions across three continents," *Proc. Nat. Acad. Sci. United States Amer.*, vol. 108, no. 24, pp. 9899–9904, Jun. 2011.

[4] T. Le Toan, S. Quegan, M. Davidson, H. Balzter, P. Paillou, K. Papathanassiou, S. Plummer, F. Rocca, S. Saatchi, H. Shugart, and L. Ulander, "The BIOMASS mission: Mapping global forest biomass to better understand the terrestrial carbon cycle," *Remote Sens. Environ.*, vol. 115, no. 11, pp. 2850–2860, Nov. 2011.

[5] Y. Pan, R. A. Birdsey, J. Fang, R. Houghton, P. E. Kauppi, W. A. Kurz, O. L. Phillips, A. Shvidenko, S. L. Lewis, J. G. Canadell, P. Ciais, R. B. Jackson, S. W. Pacala, A. D. McGuire, S. Piao, A. Rautiainen, S. Sitch, and D. Hayes, "A large and persistent carbon sink in the world's forests," *Science*, vol. 333, no. 6045, pp. 988–993, Aug. 2011.

[6] *Report for Mission Selection: BIOMASS.* (2012) [Online]. Available: http://esamultimedia.esa.int/docs/EarthObservation/SP1324-1_BIOMASSr.pdf

[7] T. Le Toan, A. Beaudoin, J. Riom, and D. Guyoni, "Relating forest biomass to SAR data," *IEEE Trans. Geosci. Remote Sens.*, vol. 30, no. 2, pp. 403–411, Mar. 1992.

[8] G. Sandberg, L. M. H. Ulander, J. E. S. Fransson, J. Holmgren, and T. L. Toan, "L- and P-band backscatter intensity for biomass retrieval in hemiboreal forest," *Remote Sens. Environ.*, vol. 115, no. 11, pp. 2874–2886, Nov. 2011.

[9] S. Saatchi, K. Halligan, D. Despain, and R. Crabtree, "Estimation of forest fuel load from radar remote sensing," *IEEE Trans. Geosci. Remote Sens.*, vol. 45, no. 6, pp. 1726–1740, Jun. 2007.

[10] M. L. Imhoff, "Radar backscatter and biomass saturation: Ramification for global biomass inventory," *IEEE Trans. Geosci. Remote Sens.*, vol. 33, no. 2, pp. 511–518, Mar. 1995.

[11] K. Papathanassiou and S. Cloude, "Single-baseline polarimetric SAR interferometry," *IEEE Trans. Geosci. Remote Sens.*, vol. 39, no. 11, pp. 2352–2363, Nov. 2001.

[12] J. Chave, C. Andalo, S. Brown, M. Cairns, J. Chambers, D. Eamus, H. Folster, F. Fromard, N. Higuchi, T. Kir, J.-P. Lescure, H. Puig, B. Riera, and T. Yamakura, "Tree allometry and improved estimation of carbon stocks and balance in tropical forests," *Oecologia*, vol. 145, no. 1, pp. 87–99, Aug. 2005.

[13] T. R. Feldpausch, J. Lloyd, S. L. Lewis, R. J. W. Brienen, M. Gloor, A. M Mendoza, G. Lopez-Gonzalez, L. Banin, K. Abu Salim, K. Affum-Baffoe, M. Alexiades, S. Almeida, I. Amaral, A. Andrade, L. E. O. C. Aragão, A. A. Murakami, E. J. M. M. Arets, L. Arroyo, G. A. C. Aymard, T. R. Baker, O. S. Bánki, N. J. Berry, N. Cardozo, J. Chave, J. A. Comiskey, E. Alvarez, A. de Oliveira, A. Di Fiore, G. Djagbletey, T. F. Domingues, T. L. Erwin, P. M. Fearnside, M. B. França, M. A. Freitas, N. Higuchi, E. Honorio, Y. Iida, E. Jiménez, A. R. Kassim, T. J. Killeen, W. F. Laurance, J. C. Lovett, Y. Malhi, B. S. Marimon, B. H. Marimon-Junior, E. Lenza, A. R. Marshall, C. Mendoza, D. J. Metcalfe, E. T. A. Mitchard, D. A. Neill, B. W. Nelson, R. Nilus, E. M. Nogueira, A. Parada, K. S.-H. Peh, A. Pena Cruz, M. C. Peñuela, N. C. A. Pitman, A. Prieto, C. A. Quesada, F. Ramírez, H. Ramírez-Angulo, J. M. Reitsma, A. Rudas, G. Saiz, R. P. Salomão, M. Schwarz, N. Silva, J. E. Silva-Espejo, M. Silveira, B. Sonké, J. Stropp, H. E. Taedoumg, S. Tan, H. Ter Steege, J. Terborgh, M. Torello-Raventos, G. M. F. van der Heijden, R. Vásquez, E. Vilanova, V. A. Vos, L. White, S. Willcock, H. Woell, and O. L. Phillips, "Tree height integrated into pantropical forest biomass estimates," *Biogeosciences*, vol. 9, no. 8, pp. 3381–3403, 2012.

[14] G. P. Asner, G. V. N. Powell, J. Mascaro, D. E. Knapp, J. K. Clark, J. Jacobson, T. Kennedy-Bowdoin, A. Balaji, G. Paez-Acosta, E. Victoria, L. Secada, M. Valqui, and R. F. Hughese, "High-resolution forest carbon stocks and emissions in the Amazon," *Proc. Nat. Acad. Sci. United States Amer.*, vol. 107, no. 38, pp. 16738–16742, Sep. 2010.

[15] R. O. Dubayah, S. L. Sheldon, D. B. Clark, M. A. Hofton, J. B. Blair, G. C. Hurtt, and R. L. Chazdon, "Estimation of tropical forest height and biomass dynamics using lidar remote sensing at La Selva, Costa Rica," *J. Geophys. Res.*, vol. 115, no. G2, pp. 1–17, 2010.

[16] J. Van Zyl, "The effect of topography on radar scattering from vegetated areas," *IEEE Trans. Geosci. Remote Sens.*, vol. 31, no. 2, pp. 153–160, Jan. 1993.

[17] P. Melon, J. Martinez, T. Le Toan, L. Ulander, and A. Beaudoin, "On the retrieving of forest stem volume from VHF SAR data: Observation and modeling," *IEEE Trans. Geosci. Remote Sens.*, vol. 39, no. 11, pp. 2364–2372, Nov. 2001.

[18] R. Lucas, M. Moghaddam, and N. Cronin, "Microwave scattering from mixed-species forests, Queensland, Australia," *IEEE Trans. Geosci. Remote Sens.*, vol. 42, no. 10, pp. 2142–2159, Oct. 2004.

[19] M. Mariotti d'Alessandro and S. Tebaldini, "Phenomenology of P-band scattering from a tropical forest through three-dimensional SAR tomography," *Geosci. Remote Sens. Lett.*, vol. 9, no. 3, pp. 442–446, May 2012.

[20] S. Tebaldini and F. Rocca, "Multibaseline polarimetric SAR tomography of a boreal forest at P- and L-bands," *IEEE Trans. Geosci. Remote Sens.*, vol. 50, no. 1, pp. 232–246, Jan. 2012.

[21] A. Reigber and A. Moreira, "First demonstration of airborne SAR tomography using multibaseline L-band data," *IEEE Trans. Geosci. Remote Sens.*, vol. 38, no. 5, pp. 2142–2152, Sep. 2000.

[22] S. Tebaldini, "Single and multipolarimetric SAR tomography of forested areas: A parametric approach," *IEEE Trans. Geosci. Remote Sens.*, vol. 48, no. 5, pp. 2375–2387, May 2010.

[23] G. Gatti, S. Tebaldini, M. Mariotti d'Alessandro, and F. Rocca, "Algae: A fast algebraic estimation of interferogram phase offsets in space varying geometries," *IEEE Trans. Geosci. Remote Sens.*, vol. 49, no. 6, pp. 2343–2353, Dec. 2010.

[24] P. Dubois-Fernandez, T. Le Toan, J. Chave, L. Blanc, S. Daniel, H. Oriot, A. Arnaubec, F. M. Rejou-Mechain, L. Villard, Y. Lasne, and T. Koleck, "TropiSAR 2009 technical assistance for the development of airborne SAR and geophysical measurements during the TropiSAR 2009 experiment," ESA, Paris, France, ESA Rep. 22446/09/NL/CT, Feb. 2011.

[25] R. Bamler and P. Hartl, "Synthetic aperture radar interferometry," *Inv. Probl.*, vol. 14, no. 1, pp. R1–R54, 1998.

[26] F. Gini, F. Lombardini, and M. Montanari, "Layover solution in multibaseline SAR interferometry," *IEEE Trans. Aerosp. Electron. Syst.*, vol. 38, no. 4, pp. 1344–1356, Oct. 2002.

[27] X. X. Zhu and R. Bamler, "Demonstration of super-resolution for tomographic SAR imaging in urban environment," *IEEE Trans. Geosci. Remote Sens.*, vol. 50, no. 8, pp. 3150–3157, Aug. 2012.

[28] F. Lombardini and M. Pardini, "3-D SAR tomography: The multibaseline sector interpolation approach," *IEEE Geosci. Remote Sens. Lett.*, vol. 5, no. 4, pp. 630–634, Oct. 2008.

[29] S. Tebaldini and A. Guarnieri, "On the role of phase stability in SAR multibaseline applications," *IEEE Trans. Geosci. Remote Sens.*, vol. 48, no. 7, pp. 2953–2966, Jul. 2010.

[30] S. Tebaldini and F. Rocca, "On the impact of propagation disturbances on SAR tomography: Analysis and compensation," in *Proc. IEEE Radar Conf.*, May 2009, pp. 1–6.

[31] S. Tebaldini, "Algebraic synthesis of forest scenarios from multibaseline PolInSAR data," *IEEE Trans. Geosci. Remote Sens.*, vol. 47, no. 12, pp. 4132–4142, Dec. 2009.

[32] A. M. Guarnieri and S. Tebaldini, "On the exploitation of target statistics for SAR interferometry applications," *IEEE Trans. Geosci. Remote Sens.*, vol. 46, no. 11, pp. 3436–3443, Nov. 2008.

[33] A. Ferretti, C. Prati, and F. Rocca, "Permanent scatterers in SAR interferometry," *IEEE Trans. Geosci. Remote Sens.*, vol. 39, no. 1, pp. 8–20, Jan. 2001.

[34] P. A. Rosen, S. Hensley, E. Gurrola, F. Rogez, S. Chan, J. Martin, and E. Rodriguez, "SRTM C-band topographic data: Quality assessment and calibration activities," in *Proc. Int. Geosci. Remote Sens. Symp.*, Jul. 2001, pp. 739–741.

[35] R. K. Raney, T. Freeman, R. W. Hawkins, and R. Bamler, "A plea for radar brightness," in *Proc. Int. Geosci. Remote Sens. Symp.*, Pasadena, CA, USA, Aug. 1994, pp. 1090–1092.

[36] R. F. Hanssen, *Radar Interferometry: Data Interpretation and Error Analysis*. New York, USA: Springer-Verlag, 2005.

[37] S. Tebaldini and F. Rocca, "Bio SAR 2008 technical assistance for the development of airborne SAR and geophysical measurements during the BioSAR 2008 experiment," ESA, Paris, France, Tech. Rep. 22052/08/NL/CT, 2009.

[38] P. C. Dubois-Fernandez, T. Le Toan, S. Daniel, H. Oriot, J. Chave, L. Blanc, L. Villard, M. W. J. Davidson, and M. Petit, "The TropiSAR airborne campaign in French Guiana: Objectives, description, and observed temporal behavior of the backscatter signal," *IEEE Trans. Geosci. Remote Sens.*, vol. 50, no. 8, pp. 3228–3241, Aug. 2012.

[39] S. Gourlet-Fleury, J.-M. Guehl, and O. Laroussinie, *Ecology and Management of a Neotropical Rainforest. Lessons Drawn From Paracou, a Long-Term Experimental Resarch Site in French Guiana*. New York, USA: Elsevier, 2004.

[40] D. Epron, A. Bosc, l. D. Bona, and V. Freycon, "Spatial variation of soil respiration across a topographic gradient in a tropical rain forest in French Guiana," *J. Tropical Ecol.*, vol. 22, no. 5, pp. 565–574, Sep. 2006.

[41] J. Chave, R. Condit, S. Aguilar, A. Hernandez, S. Lao, and R. Perez, "Error propagation and scaling for tropical forest biomass estimates," *Phil. Trans. Royal Soc.*, vol. 359, no. 1443, pp. 409–420, Mar. 2004.

[42] S. Tebaldini, M. M. Alessandro, D. H. T. Minh, and F. Rocca, "P band penetration in tropical and boreal forests: Tomographical results," in *Proc. IEEE Int. Geosci. Remote Sens. Symp.*, Jul. 2011, pp. 4241–4244.

[43] H. E. Klugh, *Statistics: The Essentials for Research*. Hillsdale, NJ, USA: Lawrence Erlbaum Associates, 1986.

[44] G. Smith-Jonforsen, L. M. H. Ulander, and X. Luo, "Low VHF-band backscatter from coniferous forests on sloping terrain," *IEEE Trans. Geosci. Remote Sens.*, vol. 43, no. 10, pp. 2246–2260, Oct. 2005.

[45] L. Thirion, E. Colin, and C. Dahon, "Capabilities of a forest coherent scattering model applied to radiometry, interferometry, and polarimetry at P- and L-band," *IEEE Trans. Geosci. Remote Sens.*, vol. 44, no. 4, pp. 849–862, Apr. 2006.

[46] R. N. Treuhaft and P. R. Siqueira, "Vertical structure of vegetated land surfaces from interferometric and polarimetric radar," *Radio Sci.*, vol. 35, no. 1, pp. 141–177, 2000.

[47] R. N. Treuhaft, B. D. Chapman, J. R. dos Santos, F. G. Goncalves, L. V. Dutra, P. M. L. A. Graca, and J. B. Drake, "Vegetation profiles in tropical forests from multibaseline interferometric synthetic aperture radar, field, and lidar measurements," *J. Geophys. Res.*, vol. 114, no. D23110.

[48] R. N. Treuhaft, F. G. Gonçalves, J. B. Drake, B. D. Chapman, J. R. dos Santos, L. V. Dutra, P. M. L. A. Graça, and G. H. Purcell, "Biomass estimation in a tropical wet forest using Fourier transforms of profiles from lidar or interferometric SAR," *Geophys. Res. Lett.*, vol. 37, no. L23403.

[49] Y.-C. Lin and K. Sarabandi, "Electromagnetic scattering model for a tree trunk above a tilted ground plane," *IEEE Trans. Geosci. Remote Sens.*, vol. 33, no. 4, pp. 1063–1070, Jul. 1995.

[50] K. Sarabandi, "Scattering from dielectric structures above impedance surfaces and resistive sheets," *IEEE Trans. Antennas Propag.*, vol. 40, no. 1, pp. 67–78, Jan. 1992.

[51] J. Chave, "Study of structural, successional and spatial patterns in tropical rain forests using TROLL, a spatially explicit forest model," *Ecolog. Model.*, vol. 124, nos. 2–3, pp. 233–254, Jun. 1999.

[52] *Article 5 (Frequency Allocations) of the Radio Regulations*, ITU Standard ITU-2004, 2004.

[53] S. Tebaldini and L. Iannini, "Assessing the performance of tomographic measurements from a P-band spaceborne SAR," in *Proc. 9th Eur. Conf. Synth. Aperture Radar*, Apr. 2012, pp. 1–4.